Characteristics of turbulent heat transfer in an annulus at supercritical pressure

Peeters, Jurriaan; Pecnik, Rene; Rohde, Martin; van der Hagen, Tim; Boersma, Bendiks Jan

DOI
10.1103/PhysRevFluids.2.024602

Publication date
2017

Document Version
Final published version

Published in
Physical Review Fluids

Characteristics of turbulent heat transfer in an annulus at supercritical pressure

J. W. R. Peeters,[1,2,*] R. Pecnik,[1] M. Rohde,[2] T. H. J. J. van der Hagen,[2] and B. J. Boersma[1]
[1]*Energy Technology, Delft University of Technology, Leeghwaterstraat 39, 2628 CB Delft, the Netherlands*
[2]*Nuclear Energy and Radiation Applications, Delft University of Technology, Mekelweg 15, 2629 JB Delft, the Netherlands*
(Received 6 October 2016; published 2 February 2017)

Heat transfer to fluids at supercritical pressure is different from heat transfer at lower pressures due to strong variations of the thermophysical properties with the temperature. We present and analyze results of direct numerical simulations of heat transfer to turbulent CO_2 at 8 MPa in an annulus. Periodic streamwise conditions are imposed so that mean streamwise acceleration due to variations in the density does not occur. The inner wall of the annulus is kept at a temperature of 323 K, while the outer wall is kept at a temperature of 303 K. The pseudocritical temperature $T_{pc} = 307.7$ K, which is the temperature where the thermophysical properties vary the most, can be found close to the inner wall. This work is a continuation of an earlier study, in which turbulence attenuation due to the variable thermophysical properties of a fluid at supercritical pressure was studied. In the current work, the direct effects of variations in the specific heat capacity, thermal diffusivity, density, and the molecular Prandtl number on heat transfer are investigated using different techniques. Variations in the specific heat capacity cause significant differences between the mean nondimensionalized temperature and enthalpy profiles. Compared to the enthalpy fluctuations, temperature fluctuations are enhanced in regions with low specific heat capacity and diminished in regions with a large specific heat capacity. The thermal diffusivity causes local changes to the mean enthalpy gradient, which in turn affects molecular conduction of thermal energy. The turbulent heat flux is directly affected by the density, but it is also affected by the mean molecular Prandtl number and attenuated or enhanced turbulent motions. In general, enthalpy fluctuations are enhanced in regions with a large mean molecular Prandtl number, which enhances the turbulent heat flux. While analyzing the Nusselt numbers under different conditions it is found that heat transfer deterioration or enhancement can occur without streamwise acceleration or mixed convection conditions. Finally, through a combination of a relation between the Nusselt number and the radial heat fluxes, a quadrant analysis of the turbulent heat flux, and conditional averaging of the heat flux quadrants, it is shown that heat transfer from a heated surface depends on the density and the molecular Prandtl number of both hot fluid moving away from a heated surface as well as the thermophysical properties of relatively cold fluid moving towards it.

DOI: 10.1103/PhysRevFluids.2.024602

I. INTRODUCTION

When a liquid at supercritical pressure is heated, its behavior changes from liquidlike to gaslike behavior in a continuous manner. During the heating process, a distinct phase transition does not occur. Fluids at supercritical pressure are used in various industrial processes, ranging from refrigeration, extraction processes, and steam generators to novel nuclear reactor designs (known as either the high-performance light water reactor or the supercritical water reactor) that utilize supercritical water as a coolant.

*j.w.r.peeters@tudelft.nl

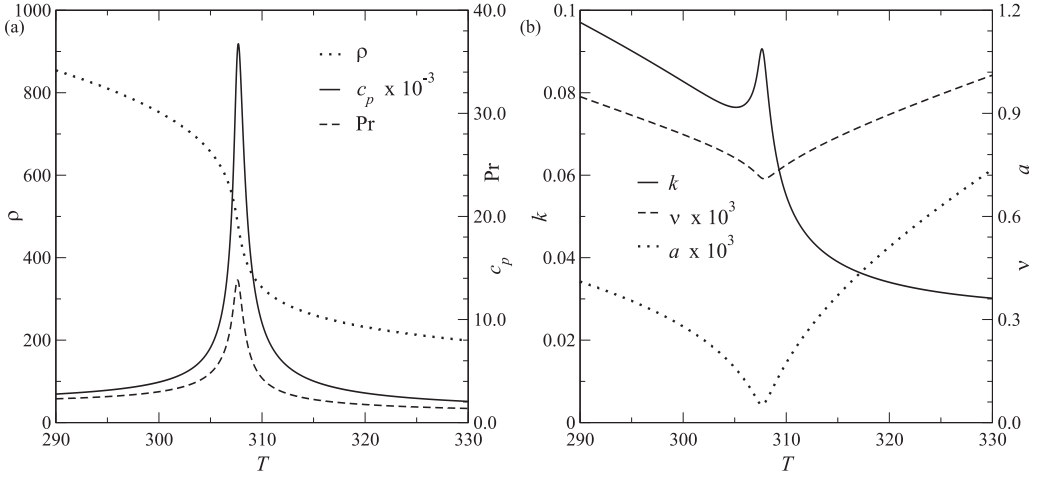

FIG. 1. Properties of CO_2 at 8 MPa as a function of the temperature T (K). Shown are the density ρ (kg/m^3), the specific heat capacity c_p (J/kg K), the molecular Prandtl number Pr (–), the thermal conductivity k (W/m K), the kinematic viscosity ν (cm^2/s), and the thermal diffusivity a (cm^2/s).

During a heating process, the thermophysical properties of a fluid at supercritical pressure will change. The most significant changes take place around the pseudocritical temperature $T_{pc} = 307.7$ K, which is defined as the temperature for which the specific heat capacity has a maximum at a given pressure, as shown in Figs. 1(a) and 1(b). The variations in the thermophysical fluid properties lead to complex heat transfer behavior; heat transfer to fluids at supercritical pressure can be enhanced or deteriorated when compared to heat transfer at subcritical pressure. This complex behavior is not well captured by standard heat transfer modeling strategies, such as turbulence modeling or Nusselt number relations; see, e.g., Refs. [1,2].

In order to develop better heat transfer models, it is necessary to understand how the variations of thermophysical properties of a fluid at supercritical pressure affect heat transfer. It is known that the production of turbulence is affected by buoyancy effects and/or acceleration effects (see Refs. [3,4]), which arise as a result of variations in density. For a comprehensive review on heat transfer at supercritical pressure see Ref. [5].

Most studies in the past have focused on the effects of buoyancy and/or streamwise acceleration, as these can lead to attenuation of the turbulent intensities and therefore attenuate mixing. The effect of buoyancy and acceleration can be regarded as indirect effects of variable density and dynamic viscosity on heat transfer, as such effects influence the flow field, which in turn affects convective heat transfer. The direct effects of variations in thermal diffusivity, specific heat capacity, density, and molecular Prandtl number are less well studied. In an earlier study, Peeters *et al.* [6], investigated how turbulence is attenuated by the variable thermophysical properties of a fluid at supercritical pressure in an annular geometry, using direct numerical simulations. In the present study, we wish to build upon that work by investigating how turbulent heat transfer is attenuated by variations of thermophysical properties at supercritical pressure conditions. Specifically, we aim to investigate the effects of variations in the specific heat capacity, thermal diffusivity, density, and molecular Prandtl number on turbulent heat transfer.

II. NUMERICAL METHODS AND CASE DESCRIPTIONS

The geometry and simulation methods were previously described in Peeters *et al.* [6]. For the sake of completeness, we will reiterate the specifics of the geometry and briefly describe the numerical methods that were used. The geometry under consideration is an annulus with an inner to outer radius ratio of 0.5. The geometry is shown in Fig. 2. The hydraulic diameter $D_h = 2R_{\text{out}} - 2R_{\text{in}}$ is equal to unity. The inner wall is kept a constant temperature of $T_h^o = 323$ K, while the outer wall is kept at

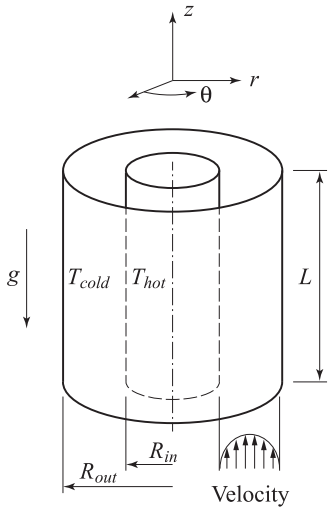

FIG. 2. The annular geometry. The inner and outer wall radii are denoted as R_{in} and R_{out}, respectively. The corresponding wall temperatures are denoted as T_{hot} and T_{cold}, respectively. The length of the annulus is denoted with L.

a temperature of $T_l^o = 303$ K. The mean temperature profile crosses the pseudocritical temperature $T_{pc} = 307.7$ K close to the inner wall. Periodic flow conditions are imposed at the inlet and the outlet.

In order to obtain nondimensional solutions for the wall normal, circumferential, and streamwise velocities, u,v,w, the hydrodynamic pressure p_{hy}, and the enthalpy h, the low Mach number approximations of the Navier-Stokes equations are solved in a numerical model:

$$\partial_t \rho + \boldsymbol{\nabla} \cdot \rho \boldsymbol{u} = 0, \tag{1}$$

$$\partial_t(\rho \boldsymbol{u}) + \boldsymbol{\nabla} \cdot (\rho \boldsymbol{u}\boldsymbol{u}) = -\nabla p_{hy} + \mathrm{Fr}^{-1} \rho \hat{\boldsymbol{z}} + \mathrm{Re}^{-1} \boldsymbol{\nabla} \cdot \{\mu(\boldsymbol{\nabla}\boldsymbol{u} + (\boldsymbol{\nabla}\boldsymbol{u})^{\mathrm{T}}) - 2/3(\boldsymbol{\nabla} \cdot \boldsymbol{u})\boldsymbol{I}\}, \tag{2}$$

and

$$\partial_t(\rho h) + \boldsymbol{\nabla} \cdot \rho \boldsymbol{u} h = (\mathrm{Re}\,\mathrm{Pr}_h)^{-1} \boldsymbol{\nabla} \cdot k \boldsymbol{\nabla} T, \tag{3}$$

where $\rho = \rho^o/\rho^o_{pc}$ is the density, $\boldsymbol{u} = \boldsymbol{u}^o/w^o_b = [u,v,w]^{\mathrm{T}}$ the velocity vector (where w^o_b is the bulk streamwise velocity), $p_{hy} = p^o_{hy}/(\rho^o_{pc} w^{o2}_b)$ the hydrodynamic pressure, $\mathrm{Fr} = w^{o2}_b/(g^o D^o_h)$, the Froude number (where g^o is the gravitational vector and D_h is the hydraulic diameter), $\hat{\boldsymbol{z}} = z/D_h$ the streamwise unit vector, $\mathrm{Re} = w^o_b D^o_h/\nu^o_{pc}$, the Reynolds number, $\mu = \mu^o/\mu^o_{pc}$ the dynamic viscosity, and $\boldsymbol{I}$ the second order unit tensor. In the last equation, $h = (h^o - h^o_l)/(h^o_h - h^o_l)$ is the enthalpy (where the subscripts h and l stand for values at the hot and cold wall, respectively), $\mathrm{Pr}_h = \mu^o_{pc}(h^o_h - h^o_l)/[k^o_{pc}(T^o_h - T^o_l)]$, the reference Prandtl number, and $T = (T^o - T^o_l)/(T^o_h - T^o_l)$, the temperature. Note that $h^o_h = h(T^o_h)$ and that $h^o_l = h(T^o_l)$. Furthermore, $(...)^o$ denotes dimensional quantities, while $(...)_{pc}$ refers to thermophysical properties at the pseudocritical temperature.

A sixth order compact finite difference method and pseudospectral methods are used to calculate spatial gradients, while a second order Adams-Bashford is employed for the time integration. The thermophysical properties density ρ, dynamic viscosity μ, and thermal conductivity k are determined using third order spline interpolations along a precomputed isobar (8 MPa) as a function of the enthalpy. The precomputed values of the thermophysical properties were calculated using equations from Refs. [7,8].

Three different numerical simulations are considered, the details of which are summarized in Table I. The results of the sCO_2 cases (II and III) will be compared against the results of the

TABLE I. Case details of numerical simulations.

Case	Properties	Pr	Flow condition	Fr^{-1}	Grid size
Reference (I)	Constant	2.85	forced convection	0	$192 \times 480 \times 512$
Forced sCO_2 (II)	sCO_2 (8 MPa)	1.6–14	forced convection	0	$256 \times 768 \times 768$
Mixed sCO_2 (III)	sCO_2 (8 MPa)	1.6–14	mixed convection	−0.1	$256 \times 768 \times 768$

reference case (I). Mixed convection conditions are only considered in the last case (III); heated upward flow occurs near the inner wall, while cooled upward flow occurs near the outer wall. In all three cases, the wall temperatures are kept constant; the inner wall is kept at $T^o = 323$ K, while the outer wall is kept at $T^o = 303$ K. In both sCO_2 cases, T_{pc} can be found close to the inner wall. The reference Prandtl number Pr_h is equal to 2.85 in all three cases. The molecular Prandtl number $\mathrm{Pr} = \mu^o c_p^o / k^o$, is equal to Pr_h in the reference case. In the sCO_2 cases, however, the molecular Prandtl number varies by an order of magnitude. The Reynolds number equals 8000 in all cases. Exact details of the grid size with respect to wall units and the Batchelor scale as well as spectra of the enthalpy fluctuations can be found in Ref. [6].

III. RESULTS

In this section we aim to characterize the differences between turbulent heat transfer in fluids at supercritical pressure and fluids with constant thermophysical properties. We will begin by discussing instantaneous visualizations of the enthalpy, temperature, and thermophysical properties in the forced convection sCO_2 case (II). Then, for each case, we will show mean statistics of the thermophysical property variations as well as the turbulent intensities. These observations are necessary for the analyses that follow thereafter.

We will first analyze the effect of the variable specific heat capacity on heat transfer by comparing the mean thermal statistics (specifically the mean enthalpy and temperature profiles, the enthalpy, and temperature rms values, as well as their respective probability density functions) between the different cases. We will proceed by analyzing how the molecular and turbulent heat fluxes are affected by the variable thermal diffusivity as well as the molecular Prandtl number. Subsequently, we will analyze the effect of the instantaneous variations of the Prandtl number and the density by using conditional averaging techniques in conjunction with a relation between the Nusselt number and the turbulent heat flux. This analysis shows how the turbulent heat flux is influenced by fluctuations of the molecular Prandtl number as well as the density.

A. Mean thermophysical property and velocity statistics

Before discussing the mean thermophysical property variations, it is convenient to write Eq. (3) completely in terms of enthalpy (see Appendix A for a derivation):

$$\partial_t(\rho h) + \nabla \cdot \rho \boldsymbol{u} h = (\mathrm{Re}\,\mathrm{Pr}_h)^{-1} \nabla \cdot \rho a \nabla h. \tag{4}$$

Equation (4) shows that the evolution of enthalpy is determined by the Reynolds and the reference Prandtl number, as well as the variations in the density and the thermal diffusivity $a \equiv k/(\rho c_p)$. The variation of the temperature can then be discussed by means of $dh = c_p dT$ (see Appendix A). Therefore, when discussing the effect of variable thermophysical properties on (turbulent) heat transfer, we will restrict the discussion to the effect of ρ,a, and c_p. The molecular Prandtl number $\mathrm{Pr} = \mu c_p / k$ will be used to discuss the transport of heat in relation to the transport of momentum.

Figure 3 (left) shows instantaneous values of the enthalpy, temperature, and specific heat capacity. The temperature fluctuations are much less apparent than the enthalpy fluctuations. Starting at the hot inner wall, the specific heat capacity is small. Farther away from it, however, c_p has a much larger value. Qualitatively, this explains why the temperature fluctuations are much less apparent than the enthalpy fluctuations; the large value of the specific heat capacity suppresses the temperature

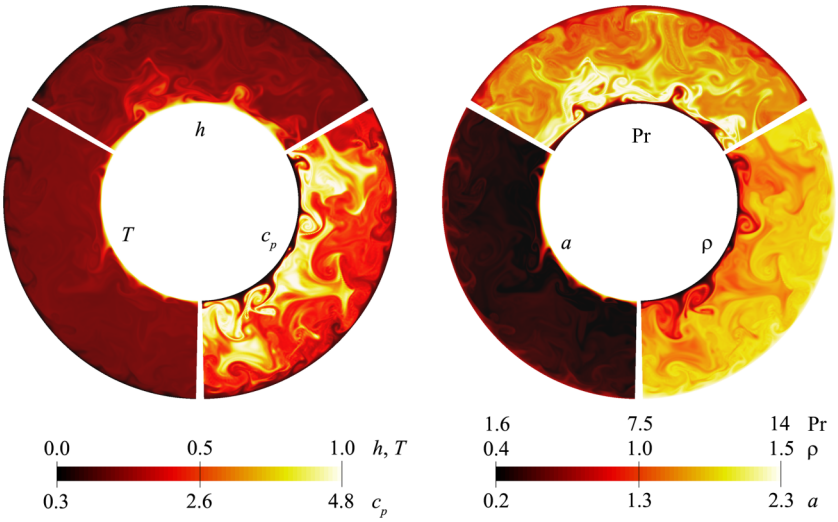

FIG. 3. Instantaneous cross-sectional visualization of thermophysical properties for the supercritical forced convection case. Left: The enthalpy, temperature, and specific heat capacity are shown. Right: The molecular Prandtl number, thermal diffusivity, and density are shown.

fluctuations. Figure 3 (right) shows instantaneous values of the thermal diffusivity, the density, and the molecular Prandtl number. Hot fluid near the inner wall has low thermal diffusivity, density, and a low Prandtl number. Especially the Prandtl number and the thermal diffusivity show large variations. The Prandtl number has a maximum quite close to the inner wall, while the thermal diffusivity has a large value at the inner wall but rapidly decreases with wall distance.

Figure 4 shows the mean variation of the density, thermal diffusivity, density, and the molecular Prandtl number near the inner (left) and the outer wall (right) as a function of the wall distance y^+, which is defined as $y^+ = (r - R_{\text{in}})/\delta_{\nu,\text{in}}$ and $y^+ = (R_{\text{out}} - r)/\delta_{\nu,\text{out}}$ for the inner and outer wall, respectively. $\delta_{\nu,\text{in}} = \mu_{w,\text{in}}/(\rho_{w,\text{in}} u_{\tau,\text{in}})$ and $\delta_{\nu,\text{out}} = \mu_{w,\text{out}}/(\rho_{w,\text{out}} u_{\tau,\text{out}})$ and $u_{\tau,\text{in}}$ and $u_{\tau,\text{out}}$ are the friction velocities at the inner and outer wall, respectively. In the following, $\widetilde{(\ldots)}$ denotes a Favre-averaged quantity, while $\overline{(\ldots)}$ denotes a Reynolds-averaged quantity. Similarly, $(\ldots)'$ denotes a fluctuation with respect to a Reynolds-averaged quantity, while $(\ldots)''$ denotes a fluctuation with

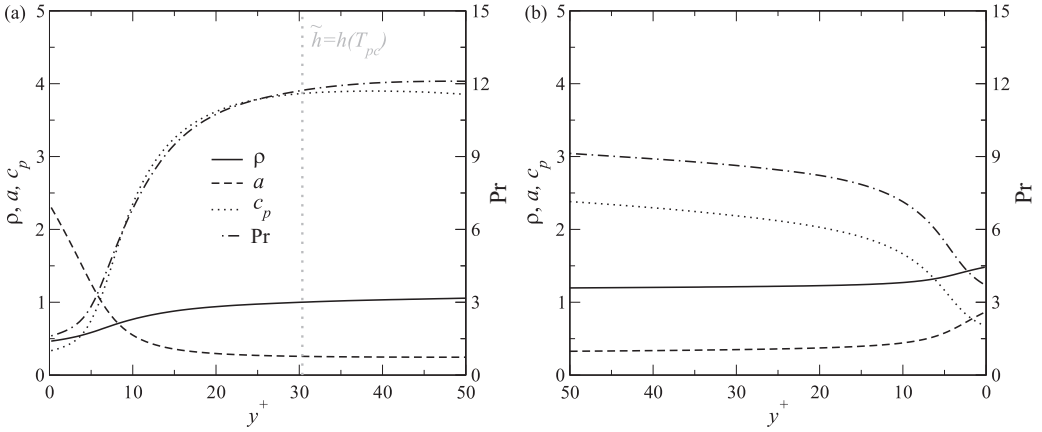

FIG. 4. Mean profiles of the density, thermal diffusivity, specific heat capacity, and molecular Prandtl number near the inner wall (a) and the outer wall (b) in the forced convection sCO_2 case (II). The vertical dotted line indicates the point where the Favre-averaged enthalpy equals the enthalpy at the pseudocritical temperature.

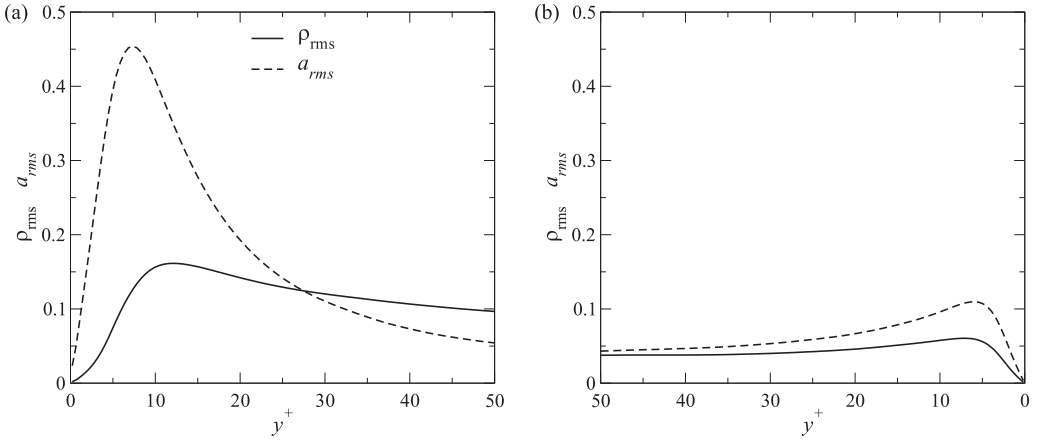

FIG. 5. Root mean square values of the density and the thermal diffusivity near the inner wall (a) and the outer wall (b) in the forced convection sCO_2 case (II).

respect to a Favre-averaged quantity. The largest mean variation of the thermophysical properties can be found near the hot inner wall for $y^+ < 20$. The mean variation is much smaller near the outer wall than it is near the inner wall. Figure 5 shows the root mean square values of the density and the thermal diffusivity near the inner wall (left) and the outer wall (right). The rms values of the thermal diffusivity are larger than the rms values of the density for $y^+ < 26$. Note that this difference stems from the fact that the thermal diffusivity and the density depend differently on the enthalpy, as was already shown in Fig. 1. Due to $\overline{\rho}$ being smaller than unity for $y^+ < 29$, the relative density fluctuation (i.e., $\rho_{\rm rms}/\overline{\rho}$) has a maximum value of 20% at $y^+ = 9.9$. Similarly, due to a being smaller than unity for $y^+ > 6.4$, the relative thermal diffusivity fluctuation ($a_{\rm rms}/\overline{a}$) has a maximum value of 80% at $y^+ = 13$. The results of the thermophysical property variations of the mixed convection case (III) are qualitatively similar to that of the forced convection case (II); these results are therefore not shown here.

The root mean square values of the velocity fluctuations, $\boldsymbol{u''} = \boldsymbol{u} - \widetilde{\boldsymbol{u}}$, of the wall normal, circumferential, and streamwise motions, denoted as $u_{\rm rms}, v_{\rm rms}, w_{\rm rms}$, respectively, for the forced convection case (II) and the mixed convection case (III), are shown in Fig. 6. Near the inner wall, the magnitude of the turbulent intensities is clearly smaller in the forced convection sCO_2 case (II) than it is in the reference case (I) for $y^+ > 7$. Near the outer wall, only $u_{\rm rms}$ and $v_{\rm rms}$ are larger in the forced convection sCO_2 case (II), but for all y^+; $w_{\rm rms}$ is near the outer wall in the forced convection sCO_2 very similar to that of the reference case. The magnitudes of $w_{\rm rms}$ and $u_{\rm rms}$ near the inner wall in the mixed convection sCO_2 case (III) are smaller than they are in the forced convection sCO_2 case (II). The magnitude of $v_{\rm rms}$ in the mixed convection case (III) is very similar to that of the forced convection case (II). The magnitude of the turbulent intensities near the outer wall in the mixed convection sCO_2 case are all larger than the magnitudes of the intensities in the reference case (I). These results show that the turbulent motions are affected by the variable properties in both sCO_2 cases, which can be traced to variable thermophysical property effects on the near wall self-regenerating cycle between streaks and quasi streamwise vortices. The observation that the momentum intensities are attenuated near the hot wall and enhanced near the outer wall will be referred to later, when investigating heat transfer characteristics.

B. Mean thermal statistics

In the previous section, we discussed that the thermophysical properties ρ, c_p, a, and Pr show large mean and instantaneous variations near the hot inner wall of the annulus. In this section,

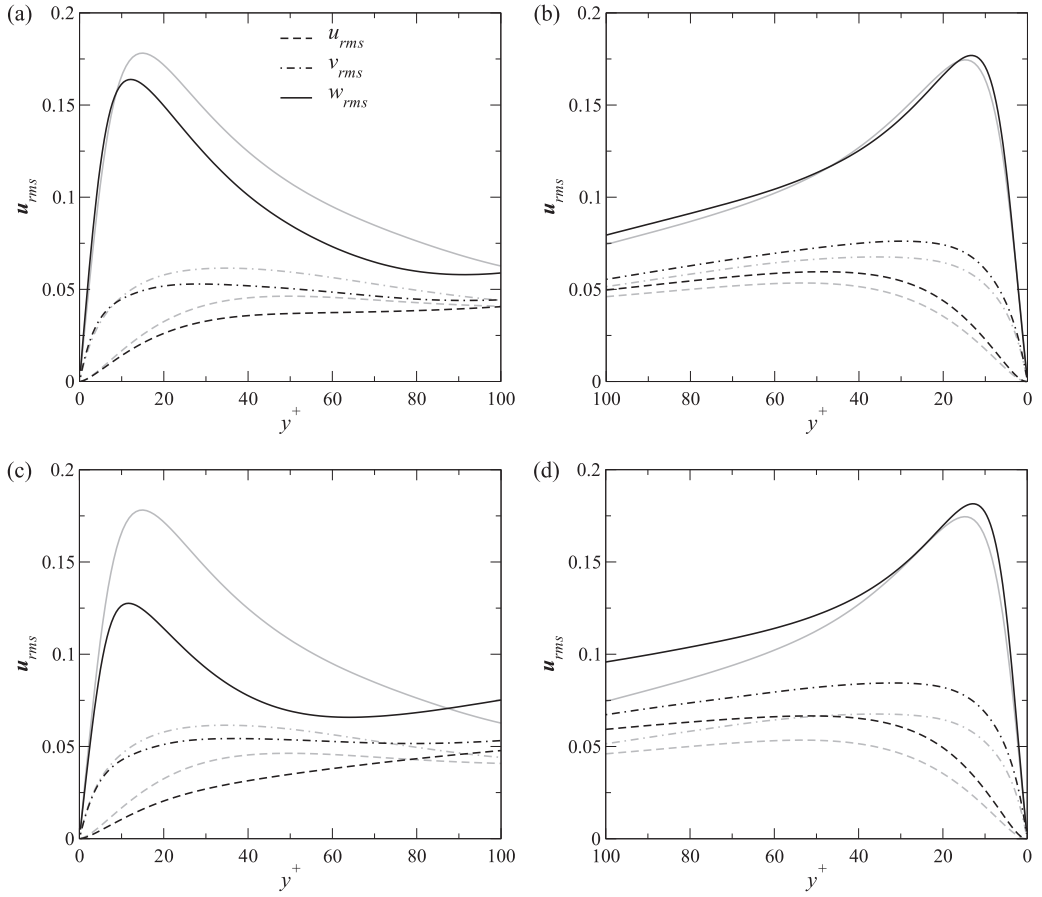

FIG. 6. Root mean square values of the velocity fluctuations. (a) forced convection sCO_2 case, inner wall region, (b) forced convection sCO_2 case, outer wall region, (c) mixed convection sCO_2 case, inner wall region, and (d) mixed convection sCO_2 case, outer wall region. The gray lines indicate rms values of the velocity fluctuations of the reference case.

we will investigate how these variations affect the mean profiles, as well as the fluctuations of the enthalpy and the temperature.

The mean enthalpy and temperature profiles for the forced convection case sCO_2 (II) and the mixed convection sCO_2 case (III) are shown in Figs. 7(a) and 7(b), respectively. The mean enthalpy values are lower for sCO_2 cases (II and III) than they are for the reference case (I), which shows that heat transfer is affected by the thermophysical property variations. This is clearer in the mixed convection sCO_2 case (III) than it is in the forced convection sCO_2 case (II). The lower values of the mean enthalpy profile in the bulk region of the sCO_2 case indicate that less heat from the wall is transported to the bulk region of the flow. This will be addressed further in Sec. III E. Very close to the inner wall, however [see the inset of Figs. 7(a) and 7(b)], the mean enthalpy values are slightly larger in the forced convection sCO_2 case than they are in the reference case.

The mean temperature values are smaller than the mean enthalpy values, which is the result of the large values of the mean specific heat capacity. Both the temperature and the enthalpy were nondimensionalized such that their values are equal to unity at the hot inner wall. Since $\partial_r T = \partial_r h / c_p$, the magnitude of the temperature must be smaller than the magnitude of the enthalpy for increasing radial distance r, as c_p is larger than unity for $y^+ > 6$.

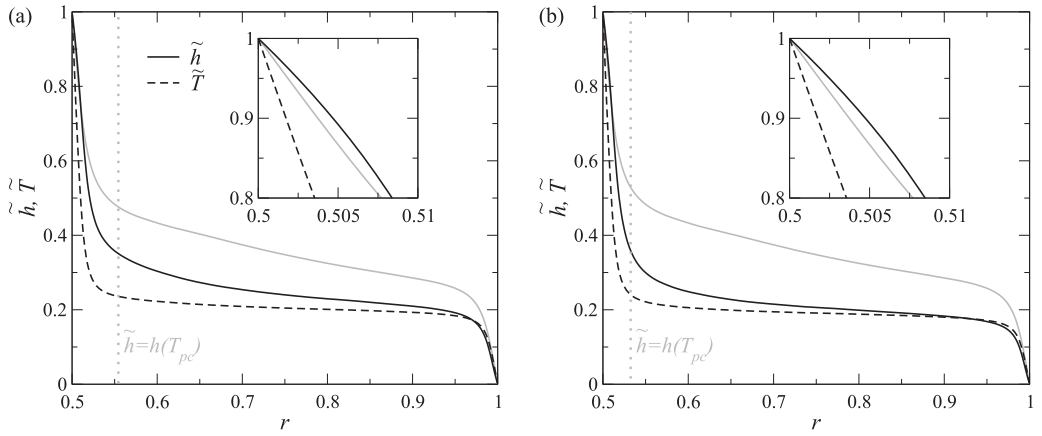

FIG. 7. Mean profiles of the enthalpy and the temperature in the forced convection sCO_2 (a) and the mixed convection sCO_2 (b) cases. The gray lines indicate results of the reference case, where $\overline{h} = \overline{T}$. The vertical dotted line indicates the point where the Favre-averaged enthalpy equals the enthalpy at the pseudocritical temperature.

Large differences are also observed in the root mean square values of the enthalpy and the temperature fluctuations, $h'' = h - \widetilde{h}$ and $T' = T - \overline{T}$. h_{rms} and T_{rms} are shown in Figs. 8(a) and 8(b) for the inner and outer wall regions, respectively. The enthalpy fluctuations are larger in the sCO_2 case than they are in the reference case (I) for $y^+ > 5$; this is typical of flows with high Prandtl numbers; see, for instance, Ref. [9]. The region where h_{rms} is larger in the sCO_2 case than it is in the reference case coincides with the region where $\overline{\mathrm{Pr}}$ is larger in the sCO_2 case than it is in the reference case. Due to the nondimensionalization of the temperature and the enthalpy, as well as the constant specific heat capacity, $T_{\mathrm{rms}} = h_{\mathrm{rms}}$ in the reference case (I). This does not hold for the sCO_2 cases. Near the inner wall, in both sCO_2 cases (II and III) [see Figs. 8(a) and 8(b)], the magnitude of h_{rms} is much larger than that of the reference case. The magnitude of T_{rms} in the sCO_2 case is larger than that of h_{rms} for $y^+ < 7.1$, but smaller for $y^+ > 7.1$ in the forced convection sCO_2 case (II). The mixed convection sCO_2 case (III) shows a similar trend. This is logical as large values of the specific heat capacity will dampen temperature fluctuations. Looking back at Fig. 4(a), $c_p < 1.0$ for $y^+ < 6.0$.

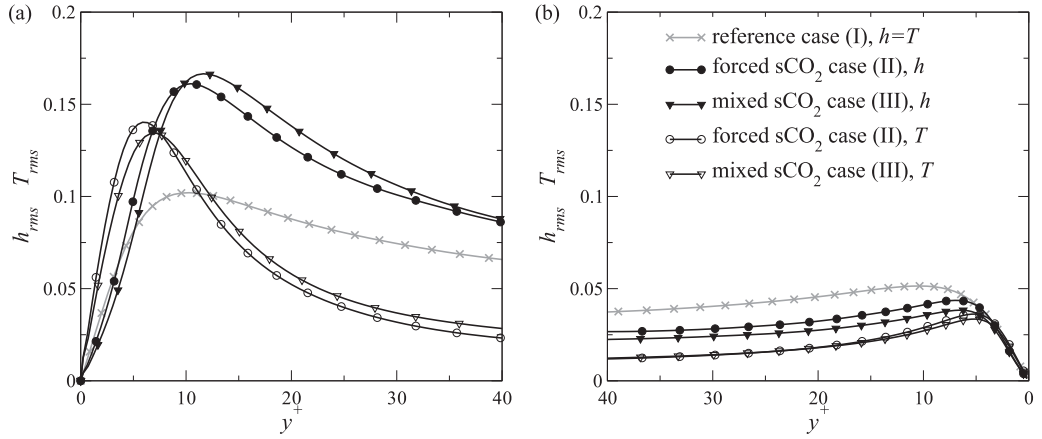

FIG. 8. Root mean square values of the enthalpy in the forced convection sCO_2 and the mixed convection sCO_2 cases near the inner wall (a) and the outer wall (b). The gray lines and crosses indicate rms values of the enthalpy in the reference case (I), where $h_{\mathrm{rms}} = T_{\mathrm{rms}}$, due to the nondimensionalization of h and T.

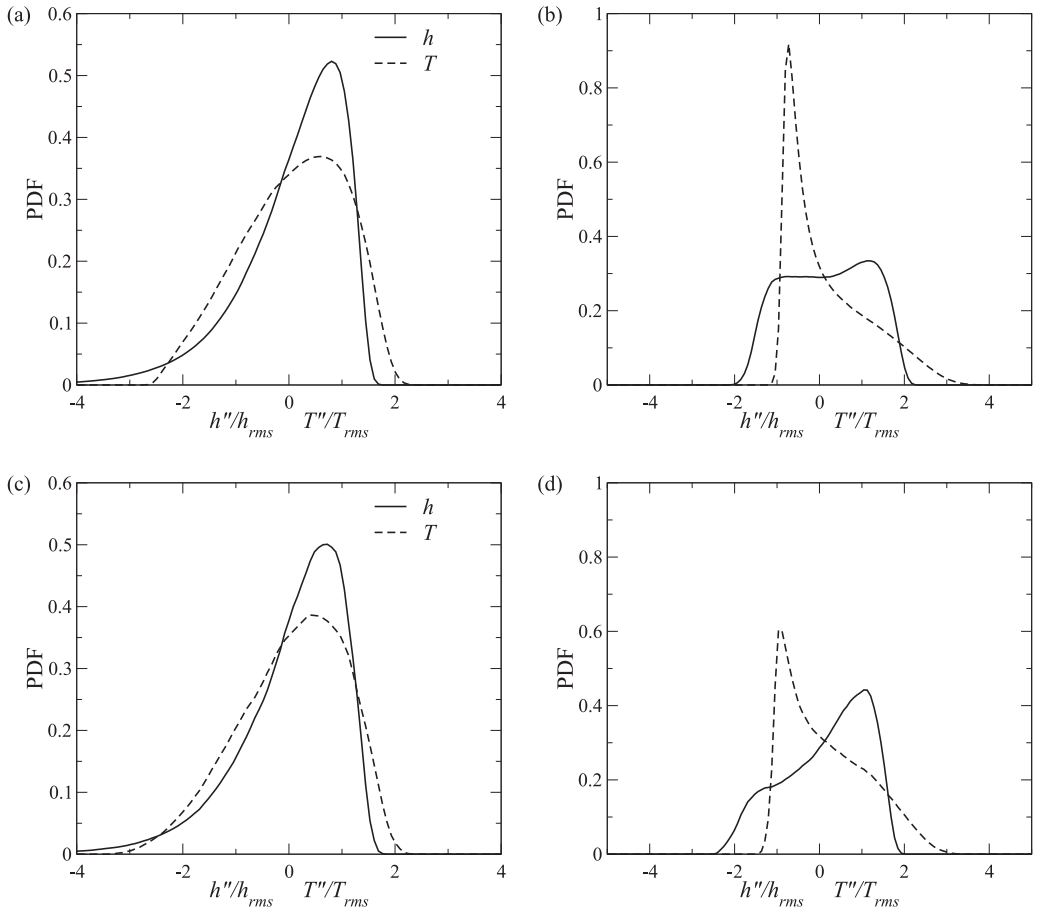

FIG. 9. Probability density functions of the enthalpy and the temperature in the forced convection sCO_2 case (II). (a) forced convection sCO_2, $y^+ = 5$, (b) forced convection sCO_2, $y^+ = 10$, (c) mixed convection sCO_2, $y^+ = 5$, and (d) mixed convection sCO_2, $y^+ = 10$.

Near the outer wall, the magnitude of T_{rms} is much smaller than that of the enthalpy as well for the sCO_2 cases for $y^+ > 4.7$, which is consistent with the fact that near the outer wall, $c_p < 1.0$ only for $y^+ < 4.0$. These findings indicate that a high average specific heat capacity dampens the magnitude of T_{rms}.

However, the previous analysis does not show how the temperature fluctuations are affected by the specific heat capacity fluctuations. To investigate the influence of the specific heat capacity fluctuations on the temperature fluctuations, probability distribution functions of the enthalpy fluctuations and the temperature fluctuations can be compared. Figures 9(a) and 9(b) show probability density functions of the enthalpy and temperature fluctuations near the inner wall at $y^+ = 5$ and $y^+ = 10$, respectively, for the forced convection sCO_2 case (II). At these locations, the average temperature is higher than the pseudocritical temperature, which means that when the enthalpy of a fluid particle increases, the specific heat capacity decreases. Vice versa, when the enthalpy decreases, the specific heat capacity increases. This means that for increasing enthalpy, the temperature increases faster due to the decrease of the specific heat capacity. This suggests that positive extreme temperature fluctuations are more likely to occur than negative extreme temperature fluctuations. This is clearly the case at $y^+ = 5$; $T' > 2T_{\mathrm{rms}}$ has a much higher probability than $h'' > 2h_{\mathrm{rms}}$, and $T' < 3T_{\mathrm{rms}}$ has a much lower probability than $h' < 3h_{\mathrm{rms}}$. At $y^+ = 10$ the differences between the probability

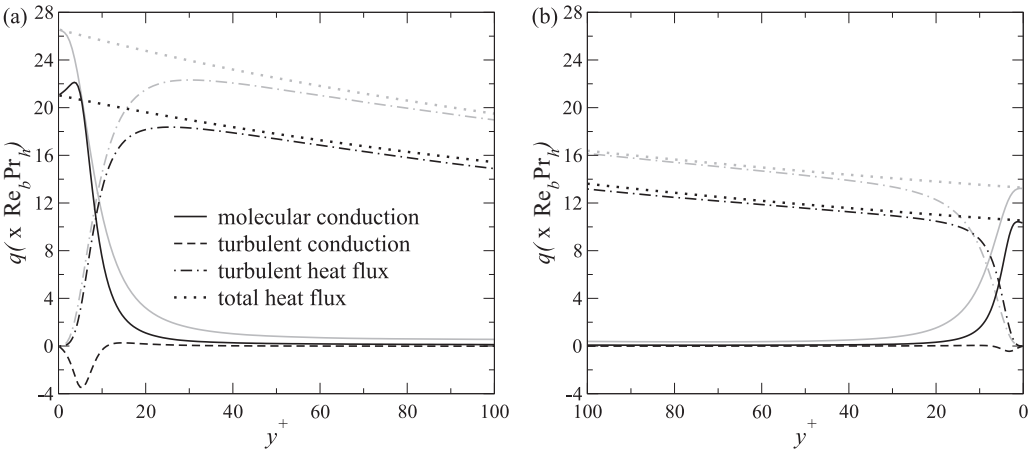

FIG. 10. Heat fluxes in the forced convection sCO_2 case (II) and the reference case (I) near the inner wall region (a) and the outer wall region (b). Gray lines indicate results of the reference case.

density distribution between the enthalpy fluctuations and the temperature fluctuations are even more apparent; $T' < T_{\mathrm{rms}}$ fluctuations are extremely unlikely, when compared to $h'' < h_{\mathrm{rms}}$ fluctuations, while $T' > 2T_{\mathrm{rms}}$ values are much more likely to occur than $h' > 2h_{\mathrm{rms}}$.

Figures 9(c) and 9(d) show the probability density functions of the enthalpy and temperature fluctuations in the mixed convection sCO_2 case (III), also at a wall distance of $y^+ = 5$ and $y^+ = 10$, respectively. The probability density functions are broader in the mixed convection sCO_2 case. This may be the result of y^+ not being the same wall distance in the mixed convection sCO_2 case (III) as it is in the forced convection case sCO_2 (II) case. Alternatively, this suggests that extreme enthalpy or temperature fluctuations are more likely in the mixed convection case than they are in the forced convection case. This can be observed for large negative fluctuations of the enthalpy or the temperature when comparing Figs. 9(c) and 9(d) with Figs. 9(a) and 9(b), respectively. This is clearest for $h''/h_{\mathrm{rms}} < 2$ when comparing Fig. 9(d) with Fig. 9(b).

C. Heat fluxes

In the previous section it was shown that the mean enthalpy has a lower magnitude in the sCO_2 cases than it has in the reference case. We argued that this is a result of less heat being transported from the hot wall towards the cold wall. We will investigate this further by looking at the heat fluxes that are present. The total heat flux q^{tot} can be written as a sum of three terms:

$$q^{\mathrm{tot}} = \overline{\rho}\widetilde{a}d_r\widetilde{h} + \overline{\rho}\widetilde{a''\partial_r h''} - \mathrm{Re}_b\mathrm{Pr}_h\overline{\rho}\widetilde{u''h''}, \tag{5}$$

where d_r is the derivative with respect to the radial direction, and ∂_r the partial derivative with respect to the same direction. The first term in Eq. (5) represents conduction, the second term a correlation between thermal diffusivity fluctuations and enthalpy gradient fluctuations, which we will refer to as *turbulent conduction*, and the last term the turbulent heat flux. The total heat flux can be expressed as $q^{\mathrm{tot}} = q_{w,\mathrm{in}}R_{\mathrm{in}}/r$, where $q_{w,\mathrm{in}} = \overline{\rho}\widetilde{a}d_r\widetilde{h}|_{r=R_{\mathrm{in}}}$. Note that the quantity $\overline{\rho}\widetilde{a}$ can qualitatively be thought of as the average thermal conductivity divided by the average specific heat capacity. The radial profiles of these fluxes are shown in Figs. 10(a) and 10(b) in the near inner and outer wall region, respectively, for the forced convection sCO_2 case.

It is clear that the total heat flux and the turbulent heat flux are smaller in the forced convection sCO_2 case, which means that less heat is transported form the hot wall to the cold wall. Molecular conduction near the inner wall shows two distinct differences when compared to the reference case (I). First, at the inner wall it is smaller than it is in the reference case (I), but, second, it increases in

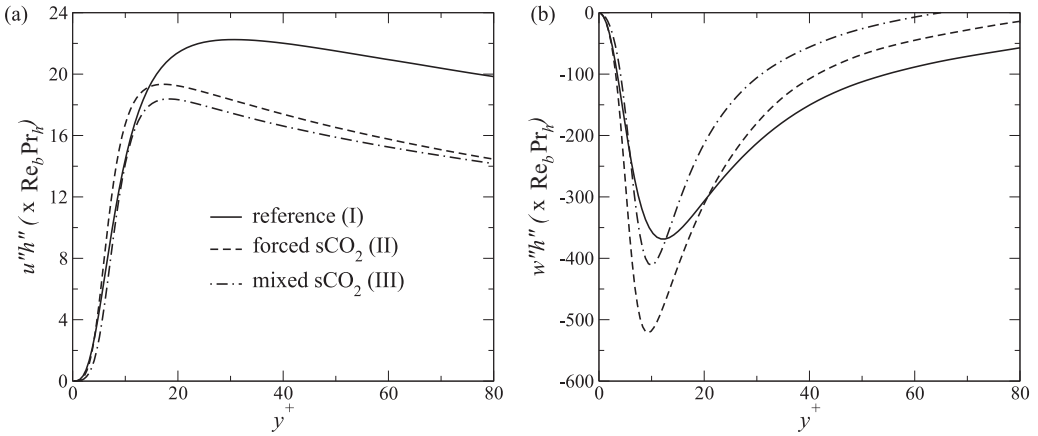

FIG. 11. The radial turbulent heat flux $\widetilde{u''h''}$ (a) and the streamwise turbulent heat flux $\widetilde{w''h''}$ (b) near the inner wall in the reference case (I), the forced convection case (II), and the mixed convection case (III).

magnitude for increasing wall distance up to $y^+ < 4$. This increase in magnitude must be the result of a relative increase in the mean enthalpy gradient, as the thermal diffusivity decreases with increasing wall distance, near the inner wall. This is in agreement with the results presented in Fig. 7(a). At $y^+ = 5$, the magnitude of molecular conduction is similar between the forced convection sCO_2 case (II) and the reference case (I). For $y^+ > 5$, molecular conduction becomes smaller again in the forced convection sCO_2 case; this can be attributed to the low values of $\overline{\rho}\widetilde{a}$. Near the outer wall, molecular conduction is smaller in the forced convection sCO_2 case than it is in the reference case for all y^+.

The heat flux by turbulent conduction is negative near both the inner wall and the outer wall, which means that, on average, it results in transport of relatively hot fluid from the bulk region towards the hot wall and relatively cold fluid from the bulk region towards the cold wall. The reason that the heat flux by turbulent conduction is negative at both walls can be explained as follows: near the inner wall, as a fluid particle heats up, the thermal diffusivity will increase as well, while near the outer wall, as a fluid particle cools down, the thermal diffusivity will decrease as well.

The fact that the turbulent heat flux is smaller in the sCO_2 forced convection case (II) than it is in the reference case (I) can be partially attributed to the low-density region near the inner wall in the sCO_2 forced convection case (II). However, the correlation $\widetilde{u''h''}$ changes as well. Figure 11(a) shows that $\widetilde{u''h''}$ is altered by the thermophysical properties of sCO_2, as well as the mixed convection condition, near the inner wall of the annulus. For $y^+ < 15$, $\widetilde{u''h''}$ is larger in the forced convection sCO_2 case (II) than it is in the reference case (I); for $y^+ > 15$, the opposite is true. $\widetilde{u''h''}$ is smaller for all y^+ in the mixed convection case (III), when compared to $\widetilde{u''h''}$ in the forced convection sCO_2 case (III), although it is almost equal to $\widetilde{u''h''}$ in the reference case up to $y^+ = 10$. Even though the wall normal velocity fluctuations are attenuated, the enthalpy fluctuations are enhanced for $y^+ > 5$, which was shown in Sec. III B. Therefore, opposing effects are here at play; the high average Prandtl number leads to large enthalpy fluctuations, but the density and dynamic viscosity variations attenuate the wall normal velocity.

Although of lesser importance to the current configuration, it is also interesting to investigate the streamwise turbulent heat flux $\overline{\rho}\widetilde{w''h''}$, which is an important quantity in configurations with thermal developing boundary layers. Near the hot wall, the correlation $\widetilde{w''h''}$ can be physically interpreted to represent near wall streaks (low speed regions, $w'' < 0$) that have a relatively high enthalpy ($h'' > 0$). Figure 11(b) shows $\widetilde{w''h''}$ near the inner wall. The magnitude of $\overline{w''h''}$ is much larger than the magnitude of $\overline{u''h''}$ close to the wall. Qualitatively, this is in line with literature; see, for instance, Refs. [10,11]. However, it should be noted here that $|\overline{w''h''}|$ is also affected by the geometry. $|\overline{w''h''}|$

is typically larger in annular geometries (close to the inner wall) than it is in channel flows; see Ref. [12,13]. Furthermore, $|\overline{w''h''}|$ increases more than $|\overline{u''h''}|$ does for increasing Prandtl numbers, according to data presented by Ref. [9] as well as Ref. [14].

$\widetilde{w''h''}$ has a larger magnitude in the forced convection sCO_2 case (II) than it has in the reference case (I). This is again the result of the larger Prandtl number, as this leads to higher enthalpy fluctuations close to the inner wall, while w_{rms} is smaller in the sCO_2 cases, near the inner wall. The streamwise turbulent heat flux is smaller in the mixed convection sCO_2 case (II) than in the forced convection sCO_2 case (III), which can be attributed to the attenuated streamwise velocity fluctuations, which are shown in Fig. 6. Thus, the same opposing effects of turbulence attenuation and enthalpy fluctuation enhancement as before with the radial turbulent heat flux are here at play.

D. Turbulent heat flux transport

To investigate the differences in $\widetilde{u''h''}$ and $\widetilde{w''h''}$ further, the transport of the turbulent heat flux can be analyzed. The transport equation of the radial turbulent heat flux can be written as

$$\begin{aligned}\overline{\rho} D_t \widetilde{u''h''} = &\underbrace{\mathrm{Re}^{-1}\overline{(\nabla\cdot 2\rho\nu h''\boldsymbol{S})_r}}_{\mathcal{D}^{\nu}_{uh}} - \underbrace{\mathrm{Re}^{-1}\overline{(2\rho\nu \boldsymbol{S}^T\cdot\nabla h'')_r}}_{\epsilon^{\nu}_{uh}}\\ &+\underbrace{(\mathrm{Re}_b\mathrm{Pr}_h)^{-1}\overline{\nabla\cdot\rho a u''\nabla h}}_{\mathcal{D}^{a}_{uh}} - \underbrace{(\mathrm{Re}_b\mathrm{Pr}_h)^{-1}\overline{\rho a(\nabla u''\cdot\nabla h'')}}_{\epsilon^{a}_{uh}}\\ &-\underbrace{r^{-1}d_r(r\overline{\rho}\widetilde{u''u''h''}) + r^{-1}\overline{\rho}\widetilde{v''^2h''}}_{\mathcal{D}^{t}_{uh}} - \underbrace{\overline{\rho}\widetilde{u''^2}d_r\widetilde{h}}_{\mathcal{P}^{th}_{uh}} - \underbrace{\overline{h''\partial_r p}}_{\Pi_{uh}},\end{aligned} \tag{6}$$

in which D_t represents the material derivative, $\boldsymbol{S} = 1/2(\nabla\boldsymbol{U} + (\nabla\boldsymbol{U})^{\mathrm{T}}) - 1/3(\nabla\cdot\boldsymbol{u})\boldsymbol{I}$, $\mathcal{D}^{t}_{uh}$ represents the turbulent mixing, $\mathcal{P}^{th}_{uh}$ thermal production, and Π_{uh} pressure scrambling. The dissipation and diffusion terms consist of a viscous part and thermal part. For the dissipation, these terms are ϵ^{ν}_{uh} and a thermal part ϵ^{a}_{uh}, and for diffusion these are $\mathcal{D}^{\nu}_{uh}$ and a $\mathcal{D}^{a}_{uh}$. Note that $\mathcal{D}^{a}_{uh}$, ϵ^{ν}_{uh}, $\mathcal{D}^{a}_{uh}$, and ϵ^{ν}_{uh} can be further decomposed, using $a = \widetilde{a} + a''$ and $\widetilde{\nu} + \nu''$. However, this is not done here, as the fluctuating thermophysical properties parts of these terms are small. An equivalent transport equation can be derived for $\widetilde{w''h''}$, the terms of which will be denoted as $(\ldots)_{wh}$. The budgets of Eq. (6) will be denoted with $\mathcal{B}(\widetilde{u''h''})$.

Figures 12(a) and 12(c) show that the thermal production $\mathcal{P}^{th}_{uh}$ is smaller in the sCO_2 cases than it is in the reference case (I); this is the result of the decreased velocity fluctuations in the wall-normal direction. The turbulent mixing term and the pressure scrambling term Π_{uh} are smaller as well. Comparing Figs. 12(a) and 12(c) reveals that the pressure scrambling term in the forced convection case is only marginally different from that in the mixed convection case. Π_{uh} can be shown to consist of four different contributions: a return-to-isotropy term, a rapid part, a buoyancy contribution, and a wall-reflection term; see, for instance, Ref. [15]. In other words, buoyancy has no direct influence on the radial turbulent heat flux. There is, however, an increase in the contribution of the viscous parts of the diffusion and dissipation terms; we will investigate this below.

The thermal part of the streamwise turbulent heat flux production, $\mathcal{P}^{th}_{wh}$, is smaller in the forced convection sCO_2 case (II) than it is in the reference case (I), as can be seen in Fig. 12(b). For $y^+ < 10$, the thermal diffusivity and dissipation contribution, which acts as a sink, is smaller in the forced convection sCO_2 case, which is the result of the low values of $\overline{\rho}\widetilde{a}$ near the inner wall. The contributions of the viscous parts of the diffusivity and dissipation are substantially smaller as well for $y^+ > 10$, which is the result of turbulence attenuation due the variation of the density and the dynamic viscosity. It follows that this analysis does not yield anymore insight into the production of $\widetilde{w''h''}$ than our analysis in Sec. III C. However, comparing the budgets of the mixed convection sCO_2 case [Fig. 12(b)] with those of the forced convection sCO_2 case [Fig. 12(d)] shows that the pressure

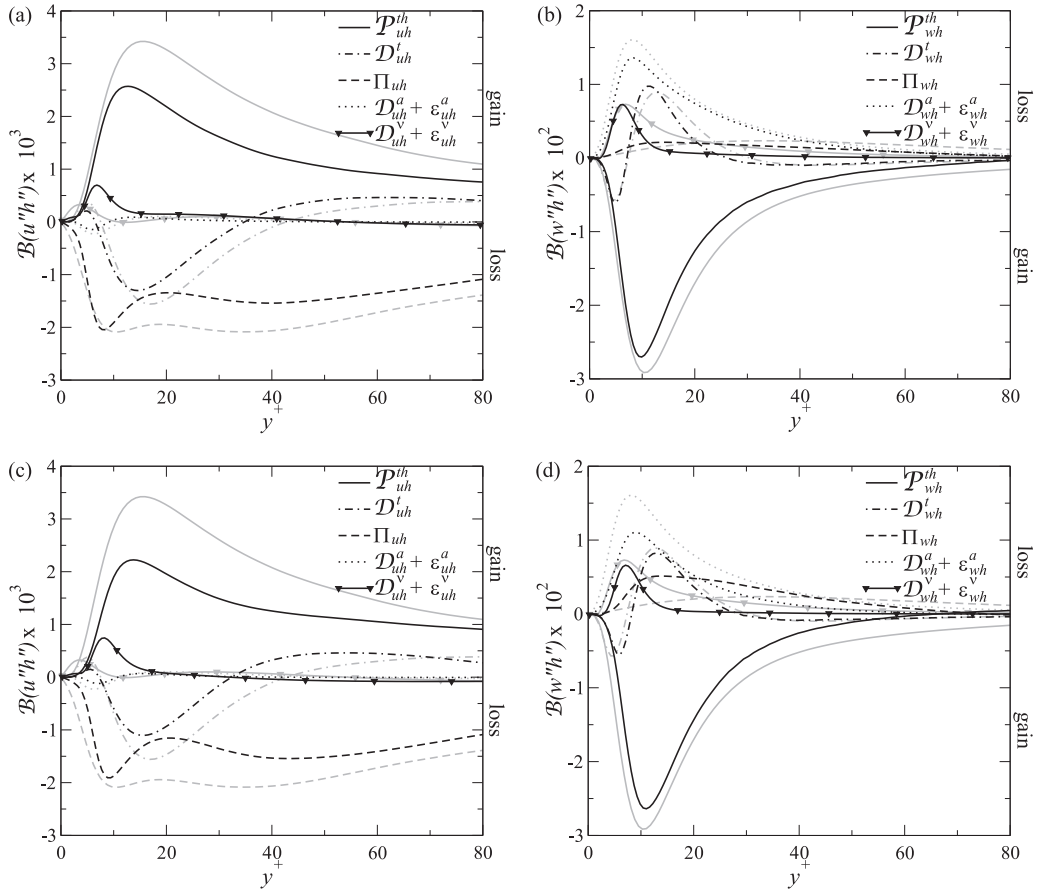

FIG. 12. Budgets of the turbulent heat flux transport equation. (a) forced convection sCO_2, radial turbulent heat flux, (b) forced convection sCO_2, streamwise turbulent heat flux, (c) mixed convection sCO_2, radial turbulent heat flux, and (d) mixed convection sCO_2, streamwise turbulent heat flux.

scrambling term is notably larger in the mixed convection sCO_2 case (III) than it is in the forced convection sCO_2 case. Thus, buoyancy influences the streamwise turbulent heat flux directly, and it has a negative effect on $\widetilde{w''h''}$ near the inner wall. This is intuitive as near wall streaks (low-speed regions) tend to have a relatively high enthalpy and therefore have a relatively low density. Similarly, a high-speed region will have a relatively low enthalpy and therefore have a high density. Peeters *et al.* [6] reasoned that, if the flow direction and the gravitational acceleration point in opposite direction, buoyancy will hamper the formation of streaks. Buoyancy therefore acts as a sink to the correlation $\widetilde{w''h''}$ through the pressure scrambling term.

We observed before that the contribution of the viscous parts of the diffusion and dissipation terms of $\mathcal{B}(\widetilde{u''h''})$ are increased in the sCO_2 cases. Figure 13 shows the viscous parts of the diffusion and dissipation terms separately for the forced convection case (II). The diffusion term in the forced convection case has shifted away from the wall, when compared to the same term in the reference case. The dissipation term is larger in the forced convection case. The increase of the dissipation term is most clear in the region $y^+ = 10$–30. This coincides with the region where $\overline{\mathrm{Pr}} > 9$ [see Fig. 4(a)], which leads to larger enthalpy fluctuations in the same region, which was already shown in Fig. 8(a). The strong correlation between the velocity gradients and the gradient of the enthalpy fluctuations is associated with the near wall turbulent structures, such as quasistreamwise vortices,

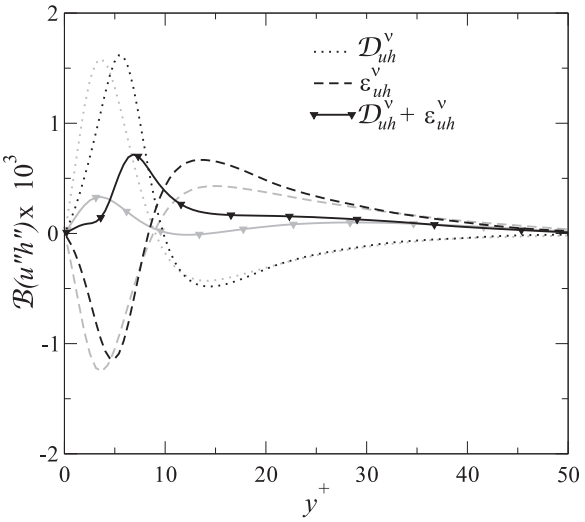

FIG. 13. Viscous parts of the diffusion and dissipation terms of the radial turbulent heat flux for reference case (I) and the forced convection sCO_2 case. The results of the reference case (I) are in gray.

streaks, and internal shear layers, which was shown in Ref. [16]. The dissipation of the turbulent heat flux is therefore increased as a result of larger instantaneous enthalpy gradients across the near wall turbulent structures.

E. Relation between the Nusselt number and the turbulent heat flux

By comparing Nusselt numbers for the hot and cold wall and for the different cases, we can determine if the local variations in thermophysical properties cause heat transfer enhancement or heat transfer deterioration. We will first define two separate Nusselt numbers for the hot and cold walls, respectively, after which we will introduce a relation between the Nusselt number and the heat fluxes as they were defined in Sec. III C. The latter will allow us to connect previous observations to changes in the Nusselt number due to variable thermophysical properties directly.

Since heating occurs at the inner wall and cooling occurs at the outer wall, we will divide the annulus into a hot side and a cold side. This will allow us to compare the effectiveness of heat transfer at both walls separately. To distinguish between the hot side and the cold side, we will choose the location where $\partial_r \widetilde{w} = 0$, denoted as $r = R_a$, to be the boundary between the hot side and the cold side. We can now define a Nusselt number for both the hot wall and the cold wall:

$$\mathrm{Nu}_h = \frac{q_w^o D_h^o}{k_{pc}^o \left(T_h^o - T_{b,h}^o\right)} \quad \text{and} \quad \mathrm{Nu}_c = \frac{q_w^o D_h^o}{k_{pc}^o \left(T_c^o - T_{b,c}^o\right)}, \tag{7}$$

where $T_{b,h}$ is the bulk temperature on the hot side and $T_{b,c}$ is the bulk temperature on the cold side. $T_{b,h}$ and $T_{b,c}$ are functions of $h_{b,h}$ and $h_{b,c}$, respectively, which in turn are defined as

$$h_{b,h} = \frac{\int_{R_{\mathrm{in}}}^{R_a} \rho w h r \, dr}{\int_{R_{\mathrm{in}}}^{R_a} \rho w r \, dr} \quad \text{and} \quad h_{b,c} = \frac{\int_{R_a}^{R_{\mathrm{out}}} \rho w h r \, dr}{\int_{R_a}^{R_{\mathrm{out}}} \rho w r \, dr}, \tag{8}$$

respectively. Fukugata *et al.* [17] showed that a relation between the Nusselt number and the heat fluxes can be derived for heated turbulent channel flows. A similar relation may be derived for the hot and cold Nusselt numbers. For the sake of readability, these derivations can be found in Appendix B.

TABLE II. Contributions to the Nusselt number at the hot inner wall.

Case	Nu_h	Molecular conduction	Turbulent conduction	Turbulent convection
Reference	41.7	5.7	–	36.0
Forced sCO_2	26.4	3.9	−0.3	22.8
Mixed sCO_2	26.2	5.3	−0.5	21.4

The relation between the hot Nusselt number and the heat fluxes can be written as

$$\mathrm{Nu}_h = \Gamma_h \Theta_h \left\{ \underbrace{\int_{R_{\mathrm{in}}}^{R_a} \overline{\rho}\widetilde{a} d_r \widetilde{h}\, dr}_{\text{molecular conduction}} + \underbrace{\int_{R_{\mathrm{in}}}^{R_a} \overline{\rho}\widetilde{a''\partial_r h''}\, dr}_{\text{turbulent conduction}} - \underbrace{\mathrm{Re}_b \mathrm{Pr}_h \int_{R_{\mathrm{in}}}^{R_a} \overline{\rho}\widetilde{u''h''}\, dr}_{\text{turbulent heat flux}} \right\}. \tag{9}$$

In this relation, the factors Γ_h and Θ_h represent a shape factor $(1/R_{\mathrm{in}})/\ln(R_{\mathrm{in}}/R_a)$ and the temperature difference ratio $(T_h - T_l)/(T_h - T_b)$, respectively. The relation for the cold Nusselt number Nu_c is simply obtained by setting R_{in} to R_{out}, Γ_h to $\Gamma_c = (1/R_{\mathrm{out}})/\ln(R_a/R_{\mathrm{out}})$ and Θ_h to $\Theta_c = (T_h - T_l)/(T_b - T_c)$. For the reference case, ρ and a are equal to unity, which may be used to reduce Eq. (9) to

$$\mathrm{Nu}_h = \Gamma_h \Theta_h \left\{ \underbrace{\widetilde{h}(R_a) - \widetilde{h}(R_{\mathrm{in}})}_{\text{molecular conduction}} - \underbrace{\mathrm{Re}_b \mathrm{Pr}_h \int_{R_{\mathrm{in}}}^{R_a} \widetilde{u''h''}\, dr}_{\text{turbulent heat flux}} \right\}. \tag{10}$$

Equations (9) and (10) are useful to determine the contribution of the different heat fluxes to the Nusselt number. These contributions are listed in Table II for the hot wall and in Table III for the cold wall, for all cases. In the reference case, the Nusselt number at the cold wall is slightly larger than the Nusselt number at the hot wall. Intuitively, this is logical as turbulence intensities near the outer wall are slightly larger than turbulence intensities near the inner wall in the reference case (I). The hot Nusselt number is smaller in the sCO_2 cases, while the cold Nusselt number is larger. At the hot side, this means that less heat is transported from the hot wall to the bulk region of the flow in the sCO_2 cases (II and III) when compared to the reference case (I), which results in a larger difference between $T_{w,h}$ and $T_{b,h}$ as was already clear from Fig. 7. The increase in the cold Nusselt number indicates that more heat is transported towards the cold wall, which results in a smaller difference $T_{w,c}$ and $T_{b,c}$, which is also visible in Fig. 7.

Qualitatively, the differences between the Nusselt numbers between the sCO_2 cases and the reference case (I) are in agreement with our earlier observations that the turbulent intensities have decreased in the sCO_2 cases near the inner wall [see Figs. 6(a) and 6(c)], but increased near the outer wall [see Figs. 6(b) and 6(d)]. However, this does not mean that the other thermophysical properties, such as the density, thermal diffusivity, and molecular Prandtl number, have no effect, as was discussed in Secs. III C and III D. Furthermore, it is also clear that the mixed convection

TABLE III. Contributions to the Nusselt number at the cold outer wall.

Case	Nu_c	Molecular conduction	Turbulent conduction	Turbulent convection
Reference	44.9	3.6	–	41.3
Forced sCO_2	52.5	2.3	0.0	50.2
Mixed sCO_2	56.5	2.3	0.0	54.2

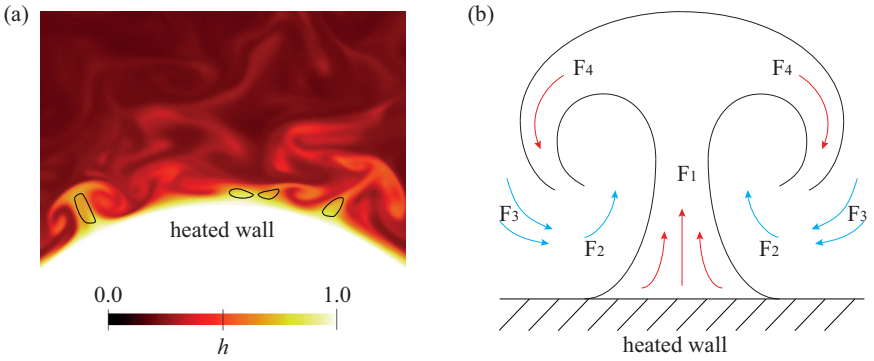

FIG. 14. (a) Typical mushroom structures near the hot wall of the annulus in the forced convection sCO_2 case. The black contour lines denote low-speed fluid regions (streaks). (b) A physical interpretation of the flux quadrants using the mushroom structure as an example.

conditions only have a small negative effect on the hot Nusselt number, but an appreciably large positive effect on the cold Nusselt number. In the mixed convection sCO_2 case (III), the contribution of the turbulent heat flux to the hot Nusselt number has decreased. However, this decrease is opposed by an increase in the molecular conduction contribution, which can only be the result of an increase of the mean enthalpy gradient (with respect to the radial distance), since the product $\overline{\rho}\widetilde{a}$ [which occurs in the first term of Eq. (9)] is smaller than unity for $y^+ > 5$. The contribution of the heat flux by turbulent conduction is negligible in all cases, both to the Nusselt number at the hot wall and that at the cold wall. Finally, the results presented in this section show that heat transfer deterioration or enhancement can occur without mean streamwise acceleration or mixed convection conditions.

F. Contributions of turbulent heat flux quadrants to the Nusselt number

The previous section gave insight into how the different heat fluxes contribute to the Nusselt number at the hot wall and the cold wall. It was shown that the variable thermophysical properties have a large effect on turbulent heat flux contribution to the Nusselt numbers. Here we will investigate the contribution of the turbulent heat flux to the Nusselt number further by making a quadrant analysis of the turbulent heat flux. For a comprehensive overview on quadrant analysis see Ref. [18]. The turbulent heat flux can be decomposed into four different terms or quadrants, which can be summarized as

(1) F_1: $u'' > 0$, $h'' > 0$, hot ejection
(2) F_2: $u'' > 0$, $h'' < 0$, cold ejection
(3) F_3: $u'' < 0$, $h'' < 0$, cold sweep
(4) F_4: $u'' < 0$, $h'' > 0$, hot sweep

Note that for determining $u'' > 0$ or $u'' < 0$, we mean to denote positive or negative radial velocity fluctuations with respect to the wall normal direction. Near the hot wall, the F_1 and F_3 quadrants yield a positive product $u''h''$, and, thus, these quadrants have a positive effect on the Nusselt number Nu_{hot}, while the F_2 and F_4 quadrants yield a negative product and thus have a negative effect. Near the cold wall, this is reversed; the F_2 and F_4 events have a positive effect, while the F_1 and F_3 have a negative effect. The turbulent heat flux quadrants can physically be interpreted as follows. Close to the hot inner wall, characteristic "mushroom" -like enthalpy (or temperature) structures can be observed, as can be seen in the top part of Fig. 3(a); this is shown more clearly in Fig. 14(a). A schematic of such a structure is shown in Fig. 14(b). The mushroom structure can be regarded as the result of the near wall cycle that exists in near wall bounded turbulence. Low-speed regions near the hot inner wall generally have a higher enthalpy than the surrounding fluid; the low-speed regions are indicated by the black contours in Fig. 14(a). Such a low-speed region grows unstable which

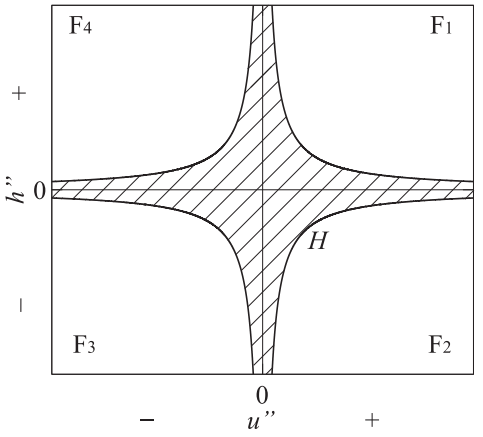

FIG. 15. Graphic representation of the hole parameter H. The "hole" is indicated by the shaded area.

results in the ejection of hot fluid [indicated in Fig. 14(b) by F_1]. The ejection leads to the formation of quasistreamwise vortices. These vortices then convect hot fluid towards the wall (indicated in the figure by F_4). These vortices also draw in relatively cold fluid from the bulk region of the flow (indicated by F_3). The inrush of cold fluid is subsequently reflected due to the presence of the wall, which results in relatively cold fluid moving away from the heated wall (indicated by F_2).

We will distinguish between small and large values of the turbulent heat flux, by defining a hole parameter H (which is similar to the approach of Willmarth and Lu [19] for the Reynolds shear stress):

$$|\rho u'' h''| > H(\overline{\rho}\widetilde{u''h''}). \tag{11}$$

The hole parameter H is a real positive number between zero and infinity. For large values of the hole parameter H, $\rho u'' h''$ represents extreme events in turbulent heat transfer, by which we mean large correlations of u'' and h''. The hole parameter is graphically represented in Fig. 15.

The integral of the radial turbulent heat flux of equation (9) can be decomposed into four terms, which represent the different flux quadrants:

$$\int_{R_{\text{in}}}^{R_a} \overline{\rho}\widetilde{u''h''}\, dr = \int_{R_{\text{in}}}^{R_a} \{(\overline{\rho}\widetilde{u''h''})_{F_1} + (\overline{\rho}\widetilde{u''h''})_{F_2} + (\overline{\rho}\widetilde{u''h''})_{F_3} + (\overline{\rho}\widetilde{u''h''})_{F_4}\} dr. \tag{12}$$

Equations (9), (11), and (12) allow us to determine the contributions of the turbulent heat flux quadrants on the Nusselt number for different values of the hole parameter H. Figures 16(a) and 16(b) show the Nusselt number contributions of the turbulent heat flux quadrants F_1–F_4 in the forced convection sCO_2 case near the hot wall and the cold wall, for the condition given by Eq. (11). Figures 17(a) and 17(b) show the same, but then for the mixed convection sCO_2 case. Figure 16(a) shows that the positive contributions to Nu_{hot}, F_1 and F_3, have substantially decreased in the forced convection sCO_2 case, when compared to the same contributions in the reference case (I). For large values of H (>8), however, the difference between the F_1 and F_3 events is very small; this is especially true for the F_3 contributions. The magnitude of the F_2 contributions has increased in the forced convection sCO_2 case, as has the magnitude of the F_4 contributions for large values of H (>4). This is surprising, because we have seen before in Fig. 6(a) that the wall normal motions have decreased in magnitude near the hot wall in the forced convection case (II), when compared to the values of the reference case (I). In other words, based purely on the observation that the magnitude of wall normal fluctuations is smaller in the sCO_2 cases, one would expect that the contribution of all flux quadrants to the Nusselt number should be smaller in the sCO_2 cases as well.

Near the cold outer wall [see Fig. 16(b)], all flux quadrant contributions to Nu_{cold}, both negative, F_1 and F_3, and positive, F_2 and F_4, have increased in magnitude. This is consistent with the fact

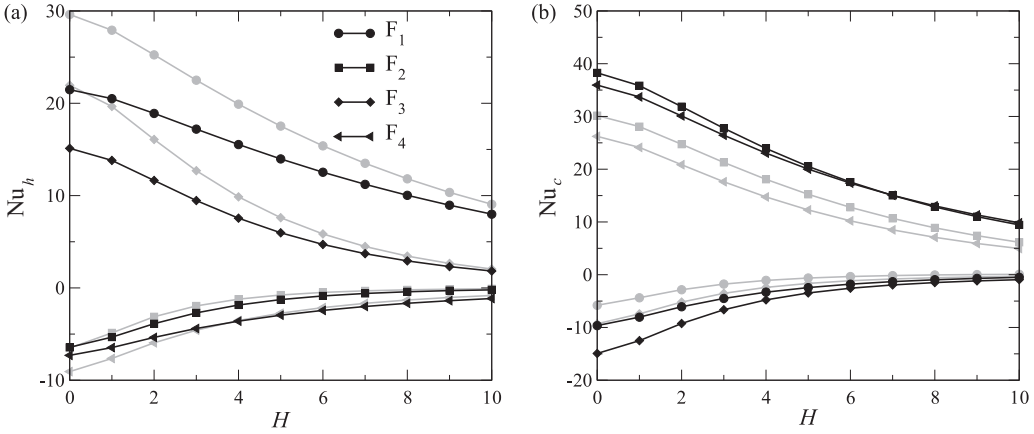

FIG. 16. Contributions of the turbulent heat flux events as a function of the hole size H in the forced convection sCO_2 case (II) (black) and the reference case (I) (gray). (a) hot inner wall, (b) cold outer wall.

that the magnitude of u'' is enhanced near the outer wall in the forced convection case (II) when compared to the same quantity in the reference case (I).

The mixed convection condition (heated, upward flow) near the hot inner wall acts as to decrease the magnitude of all the flux quadrant contributions to Nu_{hot}; this can be deduced from comparing Figs. 16(a) and 17(a). Near the outer wall, however, the mixed convection condition (cooled, upward flow) enhances the magnitude of all flux quadrant contributions to Nu_{cold}. This is consistent with our earlier observations that the magnitude of the wall-normal fluctuations near the hot wall in the mixed convection case (III) is smaller than it is in the forced convection case (II). Similarly, the increase of the flux quadrant contributions to Nu_{cold} is consistent with the increased turbulence near the outer wall.

G. Characteristics of the turbulent heat flux quadrants

It has become clear in the previous section that the turbulent heat flux quadrants near the hot inner wall in the sCO_2 cases show unexpected results that cannot be fully explained by investigating the

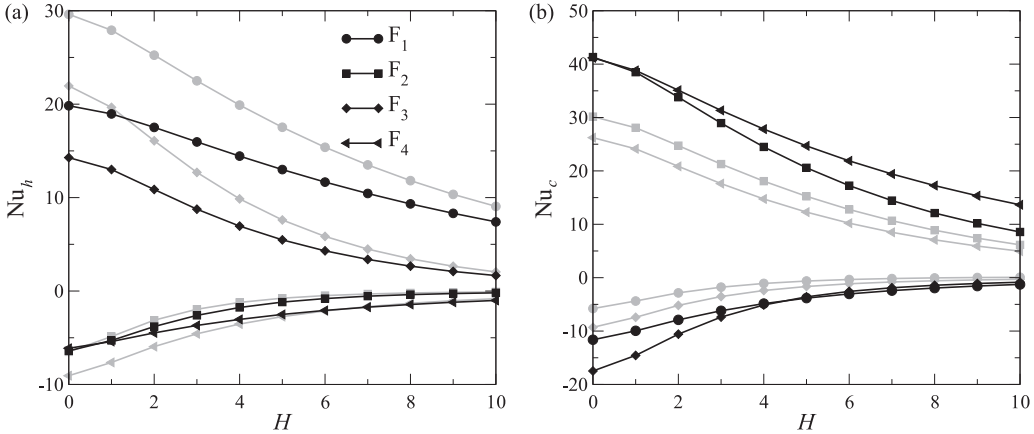

FIG. 17. Contributions of the turbulent heat flux events as a function of the hole size H in the mixed convection sCO_2 case (II) (black) and the reference case (I) (gray). (a) hot inner wall, (b) cold outer wall.

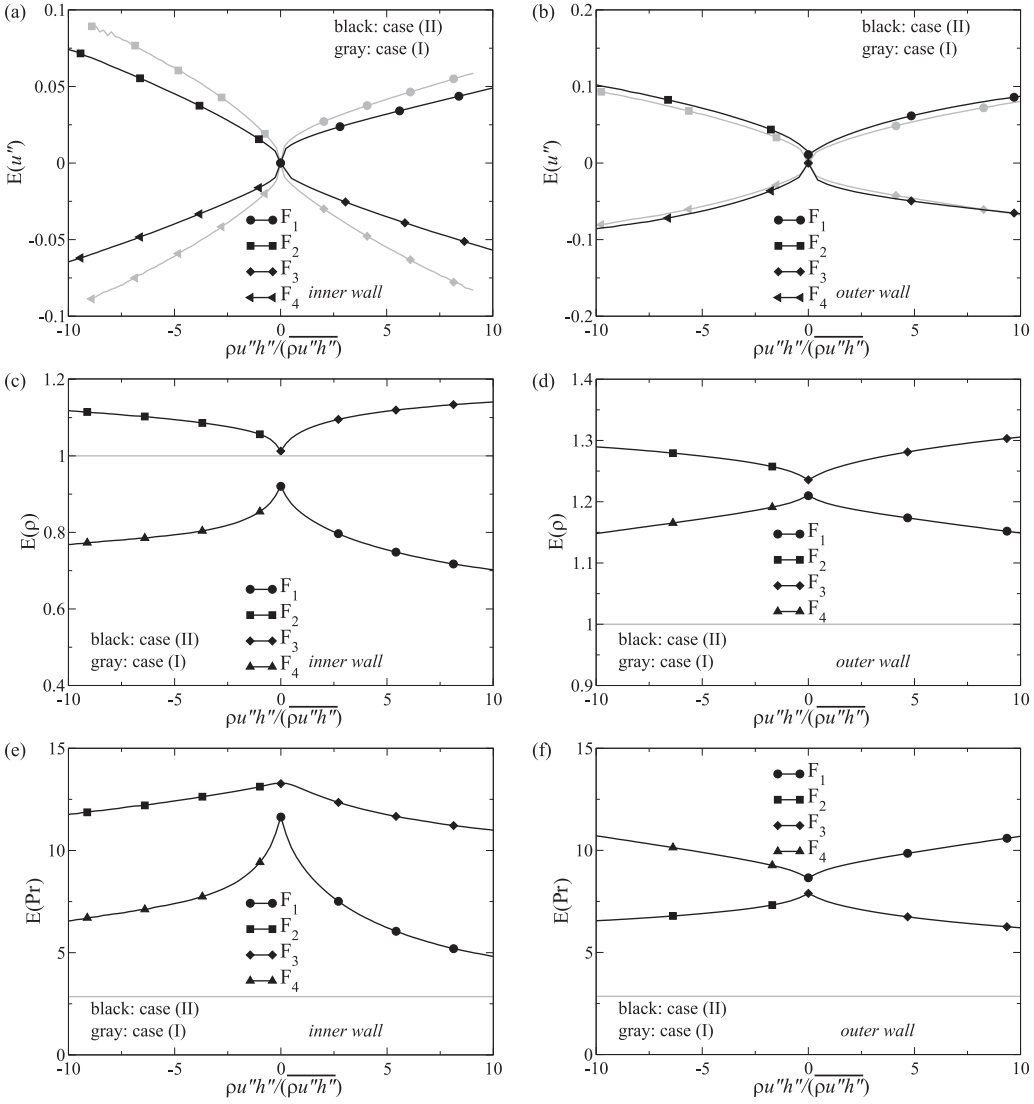

FIG. 18. Expected value of the wall normal velocity u'', the density ρ, and the molecular Prandtl number [denoted as E(u''), E(ρ), and E(Pr), respectively] conditioned on all four quadrants of the turbulent heat flux in the forced convection sCO_2 case (II) and the reference case (I) at $y^+ = 20$ near the inner wall (left column) and the outer wall (right column).

wall-normal turbulent fluctuations. We will therefore investigate how the attenuated (near the inner wall) or enhanced (near the outer wall) wall normal motions, as well as the variable thermophysical properties affect the instantaneous turbulent heat flux $\rho u''h''$. Figures 18(a) and 18(b) show the expected value of the wall normal velocity u'' near the hot inner wall and the cold outer wall (both at $y^+ = 20$). Near the hot inner wall, the magnitude of the wall normal velocity of the forced convection sCO_2 case (II) is clearly attenuated for all the flux quadrants, when compared to that of the reference case (I). The attenuation of the wall normal velocity magnitude of the F_1 quadrant is less than that of the other quadrants. Near the cold outer wall, the magnitude of the wall normal motion of the forced convection sCO_2 case is enhanced, when compared to that of the reference case (I). These findings are consistent with the results for the turbulent intensities, which were shown in Figs. 6(a) and 6(b).

The instantaneous density directly influences the magnitude of the turbulent heat flux $\rho u'' h''$. Figures 18(c) and 18(d) show the expected values of the density, $\mathrm{E}(\rho)$, conditioned on the four quadrants of the turbulent heat flux. Near the hot inner wall, the F_1 and F_4 turbulent heat flux quadrants of the forced convection sCO_2 case (II) have a low density compared to the density of the reference case (I), and the F_2 and F_3 turbulent heat flux quadrants have a higher density. The density of the F_1 quadrant is generally lower than that of the F4 quadrant. This can physically be interpreted as follows: the fluid regions that constitute the F_1 quadrant are generally hotter than the fluid regions that constitute the F_4 quadrant. Similarly, the density of the F_3 quadrant is higher than the density of F_2 quadrant, which means that fluid regions that constitute the F_3 quadrant are colder than regions that constitute the F_2 quadrant. At the outer wall, see Fig. 18(d), all turbulent heat flux quadrants in the forced sCO_2 case have a density that is higher than the density in the reference case (I). The conditional averaging analysis shows that different quadrants are affected differently by the density variations. Fluid regions with relatively low density may result in a smaller instantaneous turbulent heat flux, while regions with a high density may result in a larger instantaneous turbulent heat flux.

An interesting parameter to investigate is the time-scale ratio, which is defined as

$$R = \frac{\tau_\theta}{\tau_k} \equiv \frac{\overline{h''^2}\,\overline{\epsilon}}{2\overline{k}\,\overline{\epsilon_\theta}} = \left(\frac{\widetilde{\nu}}{\widetilde{a}}\right) \frac{\overline{h''^2}\,(\overline{2\boldsymbol{S}'' : \boldsymbol{\nabla u}''})}{\overline{k_e}\,(\overline{\boldsymbol{\nabla} h'' \cdot \boldsymbol{\nabla} h''})}, \tag{13}$$

where $\overline{\epsilon}$ is the dissipation of the turbulent kinetic energy, $\overline{\epsilon_\theta}$ the dissipation of $\overline{h''^2}$ and $\overline{k_e} = 1/2(\boldsymbol{u}'' \cdot \boldsymbol{u}'')$ the turbulent kinetic energy. This time-scale ratio can be regarded as the ratio of heat decay time to the mechanical (turbulent kinetic energy) decay time. The factor $\widetilde{\nu}/\widetilde{a}$ suggests that the time-scale ratio scales with the Prandtl number. In fact, as $y^+ \to 0$, $R \to \mathrm{Pr}$; see Refs. [9,20]. In other words, heat will decay slower than momentum in regions with high Prandtl numbers.

Figures 18(e) and 18(f) show the expected values of the molecular Prandtl number, $\mathrm{E}(\mathrm{Pr})$, conditioned on the turbulent heat flux quadrants, at the inner and outer wall, respectively. Near both walls, all turbulent heat flux quadrants have a molecular Prandtl number that is higher than the molecular Prandtl number of the reference case. Near the inner wall, the F_1 quadrant has generally a lower molecular Prandtl number than the F_4 quadrant. The same is true for the F_3 quadrant with respect to the F_2 quadrant. Near the outer wall, the F_4 and the F_1 quadrants have very similar molecular Prandtl numbers, which are lower than the molecular Prandtl number values of the F_2 and the F_3 quadrants.

To summarize, all flux quadrants are diminished by the reduced wall normal fluctuations. It is clear that all flux quadrants have different densities and molecular Prandtl numbers. The density affects the instantaneous turbulent heat flux, $\rho u'' h''$, directly, while the Prandtl number affects how fast heat will decay in comparison to how fast momentum decays. A fluid particle with a high molecular Prandtl number will convect thermal energy farther away from a hot wall, for instance, than a particle with a low molecular Prandtl number (if both particles have similar density and velocity), which will result in more effective heat transfer.

The results of the conditional averaging of the density and the molecular Prandtl number can be used to explain the differences in the turbulent heat flux quadrant contributions to the Nusselt numbers at the hot and cold walls between the sCO_2 cases and the reference case. The high Prandtl number compensates the effect of the low density and the attenuated velocity of the positive F_1 contribution and the negative F_4 contribution to Nu_h in the sCO_2 case. For the F_4 contribution, the effect of the high Prandtl number outweighs that of the attenuated velocity and the low density for large values of $\rho u'' h''$ (large H) only. The F_2 and F_3 quadrants benefit from a high density and molecular Prandtl number. For F_3, this is visible only for very high values of $\rho u'' h''$ (large H), but for F_2, the increase due the high thermophysical properties is visible for all values of $\rho u'' h''$. Near the outer wall, both positive and negative heat flux contributions to Nu_c are enhanced, as all quadrants contributions benefit from relatively high density, molecular Prandtl number, and enhanced wall normal motions. The results show that the Nusselt number is influenced by both the density and

molecular Prandtl number of relatively hot fluid as well as the density and molecular Prandtl number of relatively cold fluid.

IV. CONCLUSIONS

In this work, we have investigated characteristics of turbulent heat transfer to CO_2 at a supercritical pressure of 8 MPa in an annular geometry using direct numerical simulations. The inner wall of the annulus was kept at a temperature that is higher than the pseudocritical temperature, while the outer wall was kept at a lower temperature than the pseudocritical temperature. Results of a reference case with constant properties were compared with results of a forced convection case and a mixed convection sCO_2 case.

The variation of the thermophysical properties was found to have a large effect on mean thermal statistics. The variation of the specific heat capacity causes the mean profiles of the enthalpy and the temperature to be substantially different. High values of the specific heat capacity tend to dampen the temperature fluctuations; this is evident from both instantaneous temperature plots, as well as probability density functions of the temperature and enthalpy fluctuations. Near the hot wall, it was also found that under mixed convection conditions, the probability density functions of enthalpy and temperature fluctuations are slightly broader than under forced convection conditions.

The thermophysical properties variations also lead to a decrease in the total heat flux compared to a flow with constant thermophysical properties. The mean thermal diffusivity profile causes local changes in the mean enthalpy gradient. The turbulent conduction term, $\widetilde{\overline{\rho}a''\partial_r h''}$, that arises due to fluctuations in the thermal diffusivity and the enthalpy gradient can have a significant effect locally with respect to molecular conduction and the turbulent heat flux. The fact that the turbulent heat flux is reduced by the sCO_2 conditions cannot solely be attributed to a variation in the mean density profile, as the product of the wall-normal velocity and the enthalpy fluctuations is clearly affected by both the thermophysical property variations and the mixed convection condition. Near the hot wall, both $\widetilde{u''h''}$ and $\widetilde{w''h''}$ are modulated by two different effects. These correlations can be attenuated due to the attenuation of the turbulent intensities, which is, in turn, the result of variations in the density and the dynamic viscosity, but may also be enhanced by a high average molecular Prandtl number, which results in larger enthalpy fluctuations. While analyzing the budgets of $\widetilde{w''h''}$, it was found that the pressure-scrambling term has a significant detrimental impact on the production of the streamwise turbulent heat flux in mixed convection conditions near the hot inner wall of the annulus. Physically, this is due to the fact that buoyancy forces hinder the formation of near wall streaks.

Using a relation between the Nusselt number and the radial heat fluxes, molecular conduction, turbulent conduction, and turbulent heat flux shows that turbulent conduction, $\widetilde{\overline{\rho}a''\partial_r h''}$, has a negligible contribution to the Nusselt number, even though locally it can be significant with respect to molecular condition and the turbulent heat flux. The Nusselt number at the hot and cold walls of the forced convection sCO_2 case shows that heat transfer deterioration or enhancement can occur without mean streamwise acceleration or mixed convection conditions. Using quadrant decomposition of the turbulent heat flux, which can physically be interpreted as hot or cold fluid moving towards or away from a wall, it was found that different quadrants are affected differently by the variable thermophysical properties. Conditional averaging showed that the different heat flux quadrants have significantly different densities and molecular Prandtl numbers. This is important as fluid with high density is more effective at convecting heat than fluid with low density. High Prandtl numbers raise the heat decay time to mechanical decay time ratio; therefore, quadrants with a high molecular Prandtl number are more effective than quadrants with a low molecular Prandtl number. Therefore, different heat flux quadrants' contributions to the Nusselt number are affected differently if they have different properties. This means that the fluctuations of the density and the molecular Prandtl number are important in understanding heat transfer to fluids at supercritical pressure in addition to the mean profiles of the density and the molecular Prandtl number. Concretely, this means that heat

transfer to a fluid at supercritical pressure depends on the thermophysical properties of both the hot ejections as well as the cold sweeps.

ACKNOWLEDGMENTS

This research is supported by the Dutch Technology Foundation STW, which is part of the Netherlands Organization for Scientific Research (NWO), and which is partly funded by the Ministry of Economic Affairs.

APPENDIX A: FOURIER'S LAW IN TERMS OF THE ENTHALPY

Under the low Mach number approximation, the transport equation of the enthalpy h may be written as

$$\partial_{t^o}(\rho^o h^o) + \boldsymbol{\nabla^o} \cdot \rho^o \boldsymbol{u^o} h^o = \boldsymbol{\nabla^o} \cdot k^o \boldsymbol{\nabla^o} T^o, \tag{A1}$$

where $(...)^o$ denotes a dimensional quantity. The diffusive term can be rewritten in terms of the enthalpy by considering the following thermodynamic relations:

$$dh^o = \left(\frac{\partial h^o}{\partial T^o}\right)_{p^o} dT^o + \left(\frac{\partial h^o}{\partial p^o}\right)_{T^o} dp^o \tag{A2}$$

$$\rho^{o2}\left(\frac{\partial h^o}{\partial p^o}\right)_{T^o} = \rho^o + T^o\left(\frac{\partial \rho^o}{\partial T^o}\right)_{p^o}. \tag{A3}$$

The second of these relations is known as one of the two general thermodynamic equations of state that are valid for a system in equilibrium; see Ref. [21]. Noting that the thermal expansion coefficient at constant pressure is defined as $\beta^o = (\partial\rho^o/\partial T^o)/\rho^o$, we may write

$$dh^o = c_p^o\, dT^o + (1 + \beta^o T^o)\, dp^o/\rho^o. \tag{A4}$$

The last result can be used to write

$$\boldsymbol{\nabla^o} h^o = c_p^o \boldsymbol{\nabla^o} T^o + (1 + \beta^o T^o)\boldsymbol{\nabla^o} p^o/\rho^o. \tag{A5}$$

If the scaling, $p^o \propto \rho^o_{pc} c^{o2}$ (where c^o is the speed of sound), $\rho \propto \rho^o_{pc}$, as well as $c_p^o dT^o = w_b^{o2} c_p dT$ are used, in addition to $p = p_{th}(t) + p_{hy}(\boldsymbol{x},t)$ (where p_{th} is the thermodynamic pressure and p_{hy} the hydrodynamic pressure), the following is obtained:

$$\boldsymbol{\nabla} h = c_p \boldsymbol{\nabla} T + (1 + \beta^o T^o)\rho^{-1}\mathrm{Ma}^{-2}\boldsymbol{\nabla} p_{hy}, \tag{A6}$$

where quantities without a $(...)^o$ denote nondimensional quantities and where $\mathrm{Ma} \equiv w_b^o/c^o$ is the Mach number. Using the following scaling estimates:

$$\boldsymbol{\nabla} h \propto \frac{\Delta h}{\lambda_{th}}, \quad \boldsymbol{\nabla} T \propto \frac{\Delta T}{\lambda_{th}} \quad \text{and} \quad \boldsymbol{\nabla} p_{hy} \propto \frac{\rho w_b^2}{\mathcal{L}}, \tag{A7}$$

where $\mathcal{L}$ is the integral length scale, $\lambda_{th} \equiv \lambda/\sqrt{\mathrm{Pr}}$, the thermal equivalent of the Taylor micro scale λ, which yields

$$\Delta h \propto c_p \Delta T + w_b^2\left(\frac{1 + \beta^o T^o}{\sqrt{\mathrm{Pr}}}\right)\left(\frac{\lambda}{\mathcal{L}}\right). \tag{A8}$$

Since in a turbulent flow it holds that $\lambda/\mathcal{L} \ll 1$, the second term can be neglected, which implies that $dh \approx c_p dT$. This transforms Fourier's law into

$$q = -k\boldsymbol{\nabla} T = -\frac{k}{c_p}\boldsymbol{\nabla} h. \tag{A9}$$

APPENDIX B: DERIVATION OF THE NUSSELT NUMBER RELATION

We first define the Stanton number as $\mathrm{St} \equiv q_w^o/[\rho_{pc}^o w_b^o(h_h^o - h_l^o)]$. Decomposing all variables (except the density) of Eq. (4) and subsequently averaging the result yields

$$-r^{-1}d_r(r\overline{\rho}\widetilde{u''h''}) + (r\mathrm{Re}_b\mathrm{Pr}_h)^{-1}d_r(\overline{\rho}\widetilde{a}d_r\widetilde{h}) + (r\mathrm{Re}_b\mathrm{Pr}_h)^{-1}d_r(\overline{\rho}\widetilde{a''d_rh''}) = 0. \tag{B1}$$

Multiplying by r and integrating once, we obtain

$$-\overline{\rho}\widetilde{u''h''} + (\mathrm{Re}_b\mathrm{Pr}_h)^{-1}\overline{\rho}\widetilde{a}d_r\widetilde{h} + (\mathrm{Re}_b\mathrm{Pr}_h)^{-1}\overline{\rho}\widetilde{a''d_rh''} + \mathrm{Cr}^{-1} = 0. \tag{B2}$$

Evaluating this equation at the inner wall $r = 0.5$ and noting that the fluctuating quantities are zero at the wall, in addition that $(\mathrm{Re}_b\mathrm{Pr}_h)^{-1}\overline{\rho}\widetilde{a}d_r\widetilde{h} = (\mathrm{Re}_b\mathrm{Pr}_h)^{-1}q_w = \mathrm{St}$, gives $C = -\mathrm{St}/2$. Integrating Eq. (B2) from $r = R_{\mathrm{in}}$ to $r = R_a$, while noting that the Stanton number is constant, yields

$$\mathrm{St}\mathrm{Re}_b\mathrm{Pr}_h = \Gamma\left\{\int_{R_{\mathrm{in}}}^{R_a}\overline{\rho}\widetilde{a}\frac{d\widetilde{h}}{dr}dr + \int_{R_{\mathrm{in}}}^{R_a}\overline{\rho}\widetilde{a''\frac{dh''}{dr}}dr - \mathrm{Re}_b\mathrm{Pr}_h\int_{R_{\mathrm{in}}}^{R_a}\overline{\rho}\widetilde{u''h''}dr\right\}, \tag{B3}$$

where $\Gamma \equiv (1/R_{\mathrm{in}})/\ln(R_{\mathrm{in}}/R_a)$. Multiplying by $(T_h - T_l)/(T_h - T_b)$ yields Eq. (9).

[1] M. Sharabi and W. Ambrosini, Discussion of heat transfer phenomena in fluids at supercritical pressure with the aid of CFD models, Ann. Nuclear Energy **36**, 60 (2009).

[2] I. L. Pioro, H. F. Khartabil, and R. B. Duffey, Heat transfer to supercritical fluids flowing in channels: Empirical correlations (survey), Nucl. Eng. Des. **230**, 69 (2004).

[3] W. B. Hall and J. D. Jackson, Laminarization of a turbulent pipe flow by buoyancy forces, in 11th ASME-AIChE National Heat Transfer Conference, Minneapolis, MN, ASME paper 69-HT-55, 1969.

[4] J. D. Jackson, Fluid flow and convective heat transfer to fluids at supercritical pressure, Nucl. Eng. Des. **264**, 24 (2013).

[5] J. Y. Yoo, The turbulent flows of supercritical fluids with heat transfer, Annu. Rev. Fluid Mech. **45**, 495, (2013).

[6] J. W. R. Peeters, R. Pecnik, M. Rohde, T. H. J. J. van der Hagen, and B. J. Boersma, Turbulence attenuation in simultaneously heated and cooled annular flows at supercritical pressure, J. Fluid Mech. **799**, 505 (2016).

[7] O. Kunz, W. Wagner R. Klimeck, and M. Jaeschke, The GERG-2004 wide-range equation of state for natural gases and other mixtures, Technical report, GERG Technical Monograph 15, Fortschritt-Berichte VDI, VDI-Verlag, Düsseldorf (2007).

[8] A. Fenghour, W. A. Wakeham, and V. Vesovic, The viscosity of carbon dioxide, J. Phys. Chem. Ref. Data **27**, 31 (1998).

[9] H. Kawamura, K. Ohsaka, H. Abe, and K. Yamamoto, DNS of turbulent heat transfer in channel flow with low to medium-high Prandtl number fluid, Intl. J. Heat Fluid Flow **19**, 482 (1998).

[10] N. Kasagi and N. Shikazono, Contribution of direct numerical simulation to understanding and modeling turbulent transport, Proc. R. Soc. London A **451**, 257 (1995).

[11] H. Kong, H. Choi, and J. S. Lee, Direct numerical simulation of turbulent thermal boundary layers, Phys. Fluids **12**, 2555 (2000).

[12] S. Y. Chung and H. J. Sung, Direct numerical simulation of turbulent concentric annular pipe flow. Part II: Heat transfer, Int. J. Heat Fluid Flow **24**, 399 (2003).

[13] M. Ould-Rouiss, L. Redjem-Saad, and G. Lauriat, Direct numerical simulation of turbulent heat transfer in annuli: Effect of heat flux ratio, Intl. J. Heat Fluid Flow **30**, 579 (2009).

[14] L. Redjem-Saad, M. Ould-Rouiss, and G. Lauriat, Direct numerical simulation of turbulent heat transfer in pipe flows: Effect of Prandtl number, Intl. J. Heat Fluid Flow **28**, 847 (2007).

[15] H. S. Dol, K. Hanjalic, and T. A. M. Versteegh, A DNS-based thermal second-moment closure for buoyancy convection at vertical walls, J. Fluid Mech. **391**, 211 (1999).

[16] H. Abe, R. A. Antonia, and H. Kawamura, Correlation between small-scale velocity and scalar fluctuations in a turbulent flow, J. Fluid Mech. **627**, 1 (2009).

[17] K. Fukugata, K. Iwamoto, and N. Kasagi, Novel turbulence control strategy for simultaneously achieving friction drag reduction and heat transfer augmentation, in *Proceedings of the 4th International Symposium on Turbulence and Shear Flow Phenomena, Williamsburg, Virginia, June 27–29, 2005*, pp. 307–312.

[18] J. M. Wallace, Quadrant analysis in turbulence research: History and evolution, Annu. Rev. Fluid Mech. **48**, 131 (2016).

[19] W. W. Willmarth and S. S. Lu, Structure of the Reynolds stress near the wall, J. Fluid Mech. **55**, 65 (1972).

[20] H. Kawamura, H. Abe, and Y. Matsuo, DNS of turbulent heat transfer in channel flow with respect to Reynolds and Prandtl number effects, Intl. J. Heat Fluid Flow **20**, 196 (1999).

[21] B. Zappoli, D. Beysens, and Y. Garrabos, *Heat Transfers and Related Effects in Supercritical Fluids* (Springer, New York, 2015).